Collective-variables description of the atomic-recoil laser

Lucia De Salvo, Roberta Cannerozzi, and Rodolfo Bonifacio
Dipartimento di Fisica, Università di Milano and Istituto Nazionale di Fisica Nucleare, Via Celoria 16, 20133 Milano, Italy

Eduardo J. D'Angelo and Lorenzo M. Narducci
Physics Department, Drexel University, Philadelphia, Pennsylvania 19104
(Received 20 March 1995)

We propose a description of the collective atomic-recoil laser based on a set of nonlinear differential equations for an appropriate set of collective variables. The main obvious advantage of this description is that, when applicable, it can describe systems having an arbitrary number of particles. A comparison between the predictions of the collective equations and those of their microscopic counterparts shows a satisfactory level of accuracy, even during the nonlinear stage of the evolution. The linearized version of the collective equations is especially useful for the study of the small-signal gain or absorption spectrum and the analysis of the start-up process.

PACS number(s): 42.55.Ah, 32.80.Qk, 42.50.Vk

I. INTRODUCTION

The collective atomic-recoil laser (CARL) is a source of coherent radiation that operates as a hybrid between an ordinary laser and a free-electron laser (FEL). As originally described in Ref. [1] and further elaborated in Ref. [2], this system can be visualized as a stream of two-level atoms driven by a counterpropagating pump field and probed by a weak copropagating field whose amplification is the ultimate purpose of the device. Under appropriate conditions, the probe field can be amplified exponentially through a collective instability of the active medium leading to the spontaneous creation of a grating structure in the form of a longitudinal modulation of the atomic density [2].

The amplification process can be interpreted as the coherent backscattering of the pump field from the moving grating with an efficiency that increases as the grating structure becomes progressively better defined; it can also be interpreted in the traditional sense of pump-probe spectroscopy in which the probe samples the linear response of the driven active medium and, in the presence of gain, increases in strength [3]. In either case, the translational degrees of freedom and the internal energy levels of the atoms play an equally important role in the generation and amplification of coherent light. It is easier to appreciate this point if we picture the CARL process as the coherent backscattering of the pump wave. In fact, by virtue of the internal atomic structure, the pump field creates a macroscopic polarization within the active medium, just as in an ordinary laser. The polarization, in turn, acts as the source of a scattered field which then interferes with the pump and creates a longitudinal pendulum potential that traps and bunches the atoms. The coherent backscattered light reacts on the atoms enhances the bunching, which further increases the strength of the backscattering process, and so on. The radiation reaction originates from the collective interaction which is, ultimately, the source of the exponential gain for both the CARL and the free-electron laser. The motion of the atoms is accompanied, of course, by a Doppler shift of the scattered light. The precise connection between CARL and FEL has been analyzed in detail by Bonifacio and De Salvo in a recent contribution [4], where the common physical driving mechanism was shown to be the collective recoil-induced gain.

An important feature of ordinary laser theory is that the basic equations can be framed directly in terms of collective variables. Thus, the behavior of the individual atoms is not an important issue and the theory of the laser can readily account for a virtually arbitrary number of active units. The same does not hold, unfortunately, for the free-electron laser and CARL. During the early stages of the FEL evolution, however, its equations can be cast into an approximate form that involves collective variables [5]. Not only does this simplify the analysis of the start-up process because one is not forced to consider the evolution of a large number of individual electrons, but it also clarifies the nature of the high-gain instability in terms of the behavior of only three characteristic rate constants, i.e., the eigenvalues of the collective linear equations.

In this paper we show that also the atomic-recoil laser, for a wide range of parameters, can be described by a suitable set of collective equations during the early stages of the evolution of the system, i.e., in the linear regime. This procedure can be extended to the nonlinear part of the dynamics with the help of an approximate factorization ansatz whose purpose is to allow the derivation of a closed set of equations. Of course, the nonlinear collective equations are not exactly equivalent to the microscopic equations of Ref. [2], as one can readily expect. There is, however, a sufficiently broad range of conditions of physical interest where they provide at least a qualitatively accurate description of the amplification process, well into the saturation regime. The practical advantage of the collective equations is that they can be used to simulate the behavior of an arbitrary number of atoms

without the numerical constraints imposed by the single-particle equations. Thus, with limited effort we can derive the probe gain spectrum for short times and follow the growing influence of the atomic recoil on the evolution of the system, and the resulting departures from the standard shape of the gain spectrum of stationary driven two-level atoms. Furthermore, in the linear regime the collective equations allow the analysis of the CARL instability and of the exponential signal growth in terms of a relatively small number of eigenvalues.

The paper is organized as follows. In Sec. II we outline the derivation of the collective equations in the linear regime of the CARL model and discuss some useful consequences of this formulation. In Sec. III we extend our collective-variables description to the full nonlinear regime and compare the results of this description with those of the exact microscopic equations. We conclude this paper, in Sec. IV, with a summary of our results and some general remarks.

II. COLLECTIVE VARIABLES IN THE LINEAR REGIME

The CARL model simulates the interaction of a collection of two-level atoms with a counterpropagating pump field and copropagating optical probe. While the reader should consult Ref. [2] for a detailed description of the model, it may be useful to recall that the starting point of our analysis is provided by the traditional quantum-mechanical Hamiltonian describing the interaction of N identical two-level atoms with two counterpropagating fields. The center-of-mass motion of the atoms is accounted for by the inclusion of the standard kinetic energy term $p_j^2/2m$ for a particle with momentum p_j and mass m, and by handling the position variables z_j of each particle as the associated canonically conjugate operators.

In Refs. [1] and [2] we derived the basic equations of motion starting from the Heisenberg operator equations for the position and momentum of each atom, the creation and annihilation operators of the probe field, and the usual effective angular-momentum operators describing the atomic internal degrees of freedom (we consider the pump as a c-number driving field from the outset). After calculating the expectation values of the relevant observables in the semiclassical approximation, i.e., upon factorization of the expectation values of products of operators, the equations of motion for the scaled dimensionless variables have the explicit form

$$\frac{d\theta_j}{d\tau}=P_j \ , \tag{2.1a}$$

$$\frac{dP_j}{d\tau}=-A_1^* e^{-i\theta_j}S_j-A_1 e^{i\theta_j}S_j^*+2A_2\mathrm{Re}(S_j) \ , \tag{2.1b}$$

$$\frac{dA_1}{d\tau}=i\Delta_{21}A_1+\frac{1}{N}\sum_{j=1}^{N}S_j e^{-i\theta_j} \ , \tag{2.1c}$$

$$\frac{dS_j}{d\tau}=\frac{i}{2}(P_j+2\Delta_{20})S_j-\rho D_j(A_1 e^{i\theta_j}+A_2)-\Gamma S_j \ , \tag{2.1d}$$

$$\frac{dD_j}{d\tau}=[2\rho(A_1^* e^{-i\theta_j}+A_2)S_j+\mathrm{c.c.}]-\Gamma(D_j-1) \ , \tag{2.1e}$$

where

$$P_j=\frac{2m}{\rho\hbar(k_1+k_2)}[V_j-\bar{V}(0)] \tag{2.2a}$$

and

$$\theta_j=(k_1+k_2)[z_j-\bar{V}(0)t] \tag{2.2b}$$

are, respectively, the dimensionless momentum and position (phase) of the jth atom in the laboratory frame, $\bar{V}(0)$ is the average initial velocity of the atoms, and $k_1=\omega_1/c$ and $k_2=\omega_2/c$ are the wave numbers of the probe and pump fields, respectively. The symbol $\rho=(g_0\sqrt{n}/\omega_r)^{2/3}$ denotes the dimensionless CARL parameter; g_0 is the atom-field coupling constant ($g_0=\mu\sqrt{\omega_0/(2\hbar\varepsilon_0)}$), ω_0 is the atomic transition frequency in the rest frame of the atom, $n=N/V$ is the density of atoms in the interaction volume, $\omega_r=\hbar(k_1+k_2)^2/(2m)$ is the one-photon recoil frequency shift, and $\tau=\omega_r\rho t$ is the time scaled by the collective recoil rate $\omega_r\rho$. The scaled amplitude of the probe field is denoted by A_1, A_2 is the pump field amplitude, S_j the complex atomic polarization, and D_j is the population difference between the ground and excited states of the jth atom; finally, Γ denotes the common relaxation rate of the atomic variables S_j and D_j and the detuning parameters Δ_{21} and Δ_{20} are defined by

$$\Delta_{21}=\frac{(k_1+k_2)}{\omega_r\rho}[\bar{V}(0)-V_{r,1}], \quad \Delta_{20}=\frac{k_2}{\omega_r\rho}[\bar{V}(0)-V_{r,2}] \ , \tag{2.3a}$$

where

$$V_{r,1}=\frac{\omega_1-\omega_2}{\omega_1+\omega_2}c, \quad V_{r,2}=\frac{\omega_0-\omega_2}{\omega_2}c \ . \tag{2.3b}$$

Equations (2.1) provide a self-consistent description of the evolution of the translational and internal atomic degrees of freedom, under the action of the driving field A_2 and in the presence of the probe field A_1 whose amplification is the main objective of the study. We recognize Eqs. (2.1d) and (2.1e) as the atomic Bloch equations, suitably generalized for the inclusion of the atomic translational motion, while Eqs. (2.1a)–(2.1c) have the structure of the traditional FEL equations with additional contributions originating from the pump field and the atomic internal degrees of freedom.

The natural setting for the derivation of linearized equations involves the expansion of the dynamical variables around a suitable stationary state. The initial configuration of our system ($A_1=0$, $P_j=S_j=0$, and $D_j=1$ for all j, θ_j uniformly distributed from 0 to 2π) is not a stationary state because the atomic polarization has a nonzero rate of growth, as a result of the presence of the pump field. If Γ is not equal to zero, and if the cooling rate of the atoms under the action of the counterpropagating field is sufficiently small, a condition that is well satisfied if $\Gamma \ll \rho$ and $\Delta_{20} \gg 1$ because in this case dispersive effects dominate, the atomic momentum varies only a little from its initial value, at least during the early stages of the evolution, and the atomic variables reach a

quasisteady state in a time of the order of a few Γ^{-1}. Because of the significant lethargy in the buildup of the probe field, this nearly stationary configuration of the atomic variables persists for a long enough time (see, for example Fig. 5(d) of Ref. [2]) to justify its use as an effective initial stationary state.

Guided by these considerations, we solve Eqs. (2.1d) and (2.1e) in steady state (i.e., with $dS_j/d\tau=dD_j/d\tau=0$) and under the assumptions $|P_J| \ll |\Delta_{20}|$ and $|A_1| \ll A_2$, which are appropriate during the early stage of the evolution, and find

$$S_j=-\rho A_2\frac{\Gamma+i\Delta_{20}}{\Gamma^2+\Delta_{20}^2+4\rho^2A_2^2}\equiv S_0 , \tag{2.4a}$$

$$D_j=\frac{\Gamma^2+\Delta_{20}^2}{\Gamma^2+\Delta_{20}^2+4\rho^2A_2^2}\equiv D_0 . \tag{2.4b}$$

We now consider the following "initial" conditions:

$$\begin{aligned}&\theta_j(0)=\text{uniform},\quad P_j(0)=0,\quad A_1(0)=0 ,\\ &S_j(0)=S_0,\quad D_j(0)=D_0 ,\end{aligned} \tag{2.5}$$

and introduce the set of small fluctuation variables $\delta X_j(\tau)$, where X stands for θ, P, S, or D, according to the definitions

$$\theta_j(\tau)=\theta_j(0)+\delta\theta_j(t) , \tag{2.6a}$$

$$P_j(\tau)=\delta P_j(t) , \tag{2.6b}$$

$$S_j(\tau)=S_0+\delta S_j(t) , \tag{2.6c}$$

$$D_j(\tau)=D_0+\delta D_j(t) . \tag{2.6d}$$

At the same time, we assume that A_1 remains small enough to justify the linearization of the equations of motion (2.1).

After substituting Eqs. (2.6) and (2.4) into Eqs. (2.1) and retaining only the terms linear in the fluctuation variables, the linearized equations take the form

$$\frac{d}{d\tau}\delta\theta_j=\delta P_j , \tag{2.7a}$$

$$\frac{d}{d\tau}\delta P_j=-S_0A_1^*e^{-i\theta_j(0)}-S_0^*A_1e^{i\theta_j(0)}+2A_2S_{0x}+2A_2\delta S_{jx} , \tag{2.7b}$$

$$\frac{d}{d\tau}A_1=i\Delta_{21}A_1-iS_0\sum_{j=1}^{N}\delta\theta_je^{-i\theta_j(0)} , \tag{2.7c}$$

$$\frac{d}{d\tau}\delta S_j=\frac{i}{2}S_0\delta P_j+i\Delta_{20}\delta S_j-\rho D_0A_1e^{i\theta_j(0)}-\rho A_2\delta D_j-\Gamma\delta S_j , \tag{2.7d}$$

$$\frac{d}{d\tau}\delta D_j=2\rho(S_0A_1^*e^{-i\theta_j(0)}+A_2\delta S_j+\text{c.c.})-\Gamma\delta D_j , \tag{2.7e}$$

where we have used the notations

$$S_0=S_{0x}+iS_{0y} , \tag{2.8a}$$

$$\delta S_j=\delta S_{jx}+i\delta S_{jy} . \tag{2.8b}$$

It is now a simple matter to verify that Eqs. (2.7) together with the following definitions of the collective variables,

$$\begin{aligned}&X=\frac{1}{N}\sum_{j=1}^{N}\delta S_{jx}e^{-i\theta_j(0)},\quad Y=\frac{1}{N}\sum_{j=1}^{N}\delta S_{jy}e^{-i\theta_j(0)} ,\\ &V=\frac{1}{N}\sum_{j=1}^{N}\delta\theta_je^{-i\theta_j(0)},\quad W=\frac{1}{N}\sum_{j=1}^{N}\delta P_je^{-i\theta_j(0)} ,\\ &Z=\frac{1}{N}\sum_{j=1}^{N}\delta D_je^{-i\theta_j(0)} ,\end{aligned} \tag{2.9}$$

lead to the required linearized equations

$$\frac{dV}{d\tau}=W , \tag{2.10a}$$

$$\frac{dW}{d\tau}=-S_0^*A_1+2A_2X , \tag{2.10b}$$

$$\frac{dA_1}{d\tau}=i\Delta_{21}A_1-iS_0V+X+iY , \tag{2.10c}$$

$$\frac{dX}{d\tau}=-\frac{1}{2}S_{0y}W-\Delta_{20}Y-\frac{1}{2}\rho D_0A_1-\rho A_2Z-\Gamma X , \tag{2.10d}$$

$$\frac{dY}{d\tau}=\frac{1}{2}S_{0x}W+\Delta_{20}X+\frac{i}{2}\rho D_0A_1-\Gamma Y , \tag{2.10e}$$

$$\frac{dZ}{d\tau}=2\rho S_0^*A_1+4\rho A_2X-\Gamma Z . \tag{2.10f}$$

In arriving at Eqs. (2.10) we have used the simple relations

$$\frac{1}{N}\sum_{j=1}^{N}\cos\theta_j(0)e^{-i\theta_j(0)}=\frac{1}{2} , \tag{2.11a}$$

$$\frac{1}{N}\sum_{j=1}^{N}\sin\theta_j(0)e^{-i\theta_j(0)}=-\frac{i}{2} , \tag{2.11b}$$

which are valid if $\theta_j(0)$ is uniformly distributed, and can be proved trivially in the continuum limit $\theta_j\to\theta$, with $0\le\theta<2\pi$. We note that the first three of Eqs. (2.10) are the standard linearized FEL equations after ignoring the terms $2A_2X$ in Eq. (2.10b) and $(X+iY)$ in Eq. (2.10c). Of course, these are precisely the terms that are responsible for the coupling of the external (FEL-like) to the internal (laserlike) degrees of freedom and that eventually lead to the effects that are typical of CARL.

A convenient way to gain a global overview of the short-time behavior of the system is to display the dependence of the small-signal gain upon the frequency detuning parameter Δ_{21}. For this purpose, we define the small-signal gain (or gain spectrum) as

$$G(\Delta_{21},\tau)=\ln\left[\frac{|A_1(\tau)|^2}{|A_1(0)|^2}\right] . \tag{2.12}$$

Although this definition differs somewhat from the one introduced in Ref. [2], Eq. (3.2), we find our new choice more convenient for the purpose of comparison, when appropriate, with the Mollow spectrum of a stationary two-level atom. A typical example is shown in Fig. 1(a),

where we display the behavior of G calculated from the linearized equations (2.10) at the early time $\tau=0.5$; this figure covers a range of values of the detuning parameter Δ_{21}, which includes the absorption and Raman gain features located an effective Rabi frequency $(\Delta_{20}^2+4\rho^2 A_2^2)^{1/2}$ away from resonance, in addition to the dispersive-looking Rayleigh structure centered at the origin. These are the well known attributes of the Mollow spectrum, as pointed out in numerous earlier studies of driven two-level atoms [6]. In Fig. 1(b) we display three enlarged views of the central part of the spectrum, which is the most affected by recoil phenomena during the early part of the evolution; the three curves shown in the figure correspond to three different values of the dimensionless time τ and are matched to the corresponding solutions of the microscopic CARL equations to illustrate the typical quantitative agreement between the exact and collective short-time evolutions.

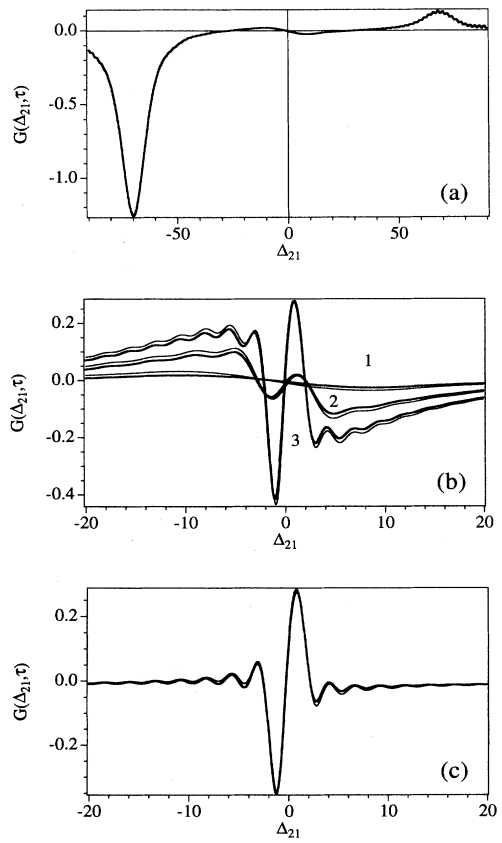

FIG. 1. (a) The gain spectrum $G(\Delta_{21},\tau)$ calculated from the linearized collective equations (2.10) at $\tau=0.5$ for the parameters $\Gamma=5$, $\rho=30$, $A_2=1$, $\Delta_{20}=-35$. (b) An enlarged view of the central part of the gain spectrum for the same values of the parameters; curve 1 corresponds to $\tau=0.5$, curve 2 to $\tau=1.5$, and curve 3 to $\tau=2.5$. The thick lines correspond to the solutions of the collective equations and the thin lines to the solutions of the exact microscopic equations (2.1). (c) The central part of the gain spectrum in the FEL limit and at $\tau=2.5$; the parameters are $\Gamma=1$, $\rho=30$, $A_2=1$, $\Delta_{20}=-120$; again, the thick line corresponds to the solutions of the collective equations and the thin line to the solutions of the exact microscopic equations (2.1).

It is important to note how the dispersionlike Raleigh part of the Mollow spectrum develops a narrow feature around $\Delta_{21}=0$ as time progresses. This typical recoil structure, which is reminiscent of the small-signal gain profile of the free-electron laser [7], here is superposed, in part, to the Rayleigh component of the Mollow spectrum. As we approach the pure FEL limit, as shown in Fig. 1(c), the Rayleigh part of the spectrum virtually disappears and the well known small-signal gain profile of the free-electron laser becomes obvious. This limit is approached by lowering the cooling rate associated with the driving field A_2 (i.e., by selecting a smaller value of the ratio Γ/ρ) and by increasing the magnitude of the detuning parameter Δ_{20}, thus decreasing the relevance of the internal atomic structure.

The results shown in Figs. 1(a)–1(c) are significant, in our opinion, because they suggest a very reasonable physical interpretation of the principles that govern the early stages of the CARL evolution. In fact, Fig. 1(a) is very reminiscent of the probe gain profile of a stationary, driven two-level atom (the so-called Mollow gain spectrum [6]). We attribute this to the fact that under the chosen conditions, the recoil does not yet play an important dynamical role. Thus, the early response of the system to a weak probe is essentially the same as the one calculated by Mollow for stationary independent atoms under true steady-state conditions. At later times the Mollow-type symmetry of the gain spectrum around $\Delta_{21}=0$ [see Fig. 1(b)] is broken, as a consequence of the effects of the recoil suffered by the atoms whose momenta are now beginning to change significantly. As time progresses further, the atomic recoil leads to the formation of the grating structure, and the small-signal gain profile becomes even more pronounced [curve 3 of Fig. 1(b)]. For even longer times, i.e., times long enough that the collective instability has had a chance to develop, the system enters a new phase of the evolution. At this point, as already shown in Ref. [2] the small-signal gain profile with its characteristic antisymmetric structure disappears and is replaced, instead, by a symmetric gain curve which is eventually responsible for the generation of the characteristic CARL exponential amplification.

The role of the atomic recoil in the CARL process can be made even more apparent if we modify artificially the linearized equations (2.10) by setting the variables V and W equal to zero, i.e., by pretending that the atoms are stationary at all times. The result, as shown in Fig. 2, is the disappearance of the antisymmetric small-signal gain structure and, for longer times, the absence of gain at $\Delta_{21}=0$, as also illustrated in Fig. 2 of Ref. [2] with the help of the exact microscopic equations.

Apart from the early appearance of the Mallow-like gain profile, which is foreign to the free-electron laser, the dynamical similarity between the linear behavior of the CARL and FEL systems can be made even more apparent if we display the real parts of the eigenvalues λ of the linearized collective equations (2.10), as shown in Fig. 3. The connection is especially striking as one compares the expanded part of this figure [see Fig. 3(b)] with Fig. 2

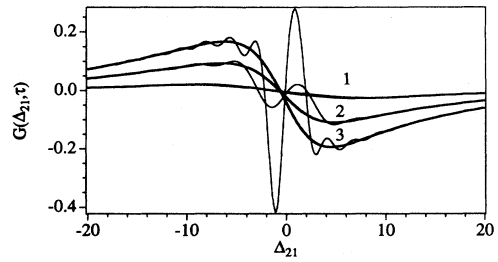

FIG. 2. The central part of the gain spectrum $G(\Delta_{21},\tau)$ calculated from the linearized collective equations for the same parameters used in Fig. 1(a). The thin lines have been obtained with the full set of equations (2.10); the thick lines correspond to the simplified collective equations after the artificial removal of the variables V and W. Curves 1, 2, and 3 correspond to the same values of τ used in Fig. 1(a).

of Ref. [5]. The qualitative similarities are obvious; here also, for example, as in the case of the free-electron laser, we recognize the existence of an instability threshold with respect to the detuning parameter Δ_{21}. When the FEL is below threshold for amplification (i.e., for $\Delta_{21}>\Delta_{21}^{\text{thr}}$, in terms of our current notations) the real parts of the eigenvalues are zero and the linearized solutions are simple oscillating functions of time, while above threshold ($\Delta_{21}<\Delta_{21}^{\text{thr}}$), the signal grows exponentially. The situation is qualitatively the same for CARL apart from some additional complications [see, for example, the region around $\Delta_{21}=0$ in Fig. 3(b)] due to the mixing of FEL-like and laserlike features. In the FEL limit (see Fig. 4) the behavior of the real part of the CARL eigenvalues is far

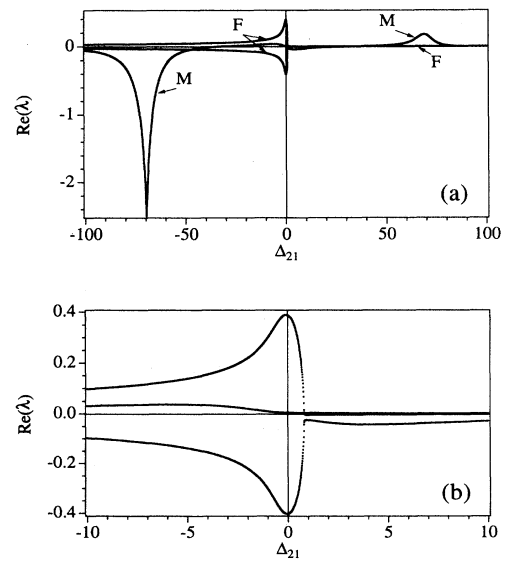

FIG. 3. (a) The three eigenvalues of the collective equations (2.10) with the largest real parts. The labels M and F refer to the parts of the curves with the same qualitative behavior as in the case of a driven stationary atom (Mollow) and in the case of FEL, respectively. (b) An enlarged view of (a) around $\Delta_{21}=0$. The parameters are the same as those used in Fig. 1(a).

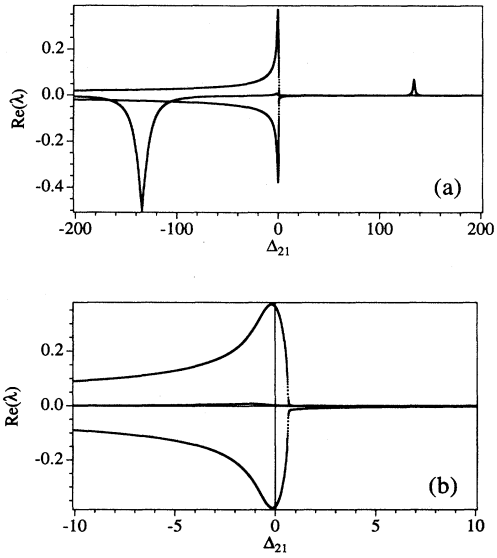

FIG. 4. (a) The three eigenvalues of the collective equations (2.10) with the largest real parts. (b) An enlarged view of (a) around $\Delta_{21}=0$. The parameters are the same as those used in Fig. 1(c).

more transparent. The Raman and absorption features are readily visible, although significantly reduced in magnitude, the Rayleigh part of the eigenvalue spectrum has almost disappeared, and the close-up of the FEL-like structure [Fig. 4(b)] looks almost exactly like Fig. 2 of Ref. [5].

III. COLLECTIVE NONLINEAR EQUATIONS

Beyond the linear regime, the simple description of the preceding section fails and a complete solution of the problem, including saturation effects, requires the numerical integration of $5N+2$ equations, where N is the number of atoms. Obviously, this is not a trivial task, especially if N is of the order of a few hundreds, or even larger. In this section we propose an approximate collective-variables description of CARL that is capable of reproducing the behavior of the exact equations with good qualitative accuracy, even in the nonlinear regime. In spite of the formal complexity of the resulting collective equations, an obvious advantage is that they can be used regardless of the number of particles.

If B_j denotes any dynamical variables related to the jth particle, we define its mean value as

$$\langle B\rangle = N^{-1}\sum_j B_j \ . \tag{3.1a}$$

Thus,

$$\langle P\rangle = N^{-1}\sum_j P_j \ , \tag{3.1b}$$

$$\langle P^2\rangle = N^{-1}\sum_j P_j^2 \ , \tag{3.1c}$$

$$\langle S\rangle = N^{-1}\sum_j S_j \ , \tag{3.1d}$$

$$\langle \Delta \rangle = N^{-1} \sum_j D_j \tag{3.1e}$$

denote, respectively, the average momentum, the kinetic energy [apart from the factor $1/(2m)$], the atomic polarization, and the population difference. In addition, we define the average complex bunching parameter [8]

$$V = \langle \exp(-i\theta_j) \rangle = N^{-1} \sum_j \exp(-i\theta_j) , \tag{3.1f}$$

whose modulus is bounded between zero and unity; the lower limit of $|V|$ corresponds to a configuration in which the particles are distributed uniformly in space, while $|V| \to 1$ signals that the particles' density displays a periodic modulation with the period of an optical wavelength, a situation that allows an efficient energy transfer from the atoms to the field.

As in Sec. II, here also it is convenient to define the variables

$$X = \langle \mathrm{Re} S_j e^{-i\theta_j} \rangle , \tag{3.2a}$$

$$Y = \langle \mathrm{Im} S_j e^{-i\theta_j} \rangle , \tag{3.2b}$$

$$Z = \langle D_j e^{-i\theta_j} \rangle , \tag{3.2c}$$

where $\mathrm{Re}S_j$ and $\mathrm{Im}S_j$ are the real and imaginary parts of the polarization of the jth atom. With the help of Eqs. (3.2), the field equation takes the form

$$\frac{dA_1}{d\tau} = iA_1\Delta_{21} + X + iY . \tag{3.3}$$

Furthermore, Eqs. (2.1) and (3.2) together yield the following evolution equations for X, Y, and Z:

$$\frac{dX}{d\tau} = -i\langle Pb\ \mathrm{Re}S \rangle - \tfrac{1}{2}\langle Pb\ \mathrm{Im}S \rangle - \Delta_{20}Y - \rho A_2 Z - \tfrac{1}{2}\rho A_1 \langle \Delta \rangle - \tfrac{1}{2}\rho A_1^* \langle Db^2 \rangle - \Gamma X , \tag{3.4}$$

$$\frac{dY}{d\tau} = -i\langle Pb\ \mathrm{Im}S \rangle + \tfrac{1}{2}\langle Pb\ \mathrm{Re}S \rangle + \Delta_{20}X + i\tfrac{1}{2}\rho A_1 \langle \Delta \rangle - i\tfrac{1}{2}\rho A_1^* \langle Db^2 \rangle - \Gamma Y , \tag{3.5}$$

$$\frac{dZ}{d\tau} = 4\rho A_2 X - \Gamma Z + 2\rho A_1^* \langle b^2 S \rangle + 2\rho A_1 \langle S^* \rangle - i\langle PbD \rangle + \Gamma V , \tag{3.6}$$

where $b_j \equiv \exp(-i\theta_j)$. The equation of motion for the average bunching parameter follows from Eqs. (3.1f) and (2.1a) and has the form

$$\frac{dV}{d\tau} = -iW . \tag{3.7}$$

where W denotes the joint phase-momentum average

$$W = \langle \exp(-i\theta) P \rangle = N^{-1} \sum_j e^{-i\theta_j} P_j . \tag{3.8}$$

From the definition (3.8) and the CARL equation (2.1b) one can easily derive the following equation of motion for W:

$$\frac{dW}{d\tau} = -i\langle P^2 b \rangle + 2A_2 X - A_1^* \langle Sb^2 \rangle - A_1 \langle S^* \rangle , \tag{3.9}$$

where, according to the definition of mean value of a dynamical variable, Eq. (3.1a), we have

$$\langle P^2 b \rangle = N^{-1} \sum_j e^{-i\theta_j} P_j^2 , \tag{3.10}$$

$$\langle Sb^2 \rangle = N^{-1} \sum_j e^{-2i\theta_j} S_j . \tag{3.11}$$

Because, in general, the equations of motion for the mean values of the product of M dynamical variables depend on mean values involving the product of $M+1$ variables, the construction of the equations of motion yields an infinite hierarchy of coupled equations, as expected. We truncate this hierarchy by assuming the (approximate) validity of the following relations:

$$\langle (P - \langle P \rangle)^2 b \rangle = \langle (P - \langle P \rangle)^2 \rangle V , \tag{3.12a}$$

$$\langle (S - \langle S \rangle) Pb \rangle = \langle (S - \langle S \rangle) b \rangle \langle P \rangle , \tag{3.12b}$$

$$\langle (S - \langle S \rangle) bb \rangle = \langle (S - \langle S \rangle) b \rangle V , \tag{3.12c}$$

whose accuracy we have tested with the help of numerical solutions of the exact equations (2.10). A sample test is shown in Fig. 5, where we analyze the behavior of the real and imaginary parts of both sides of Eq. (3.12b). Furthermore, from Eqs. (3.12) we obtain

$$\langle P^2 b \rangle = 2\langle P \rangle W + \langle P^2 \rangle V - 2\langle P \rangle^2 V , \tag{3.13}$$

$$\langle SPb \rangle = \langle P \rangle S - \langle S \rangle \langle P \rangle V + \langle S \rangle W , \tag{3.14}$$

$$\langle Sb^2 \rangle = \langle S \rangle B + SV - \langle S \rangle V^2 , \tag{3.15}$$

where $S \equiv \langle Sb \rangle$ and $B \equiv \langle b^2 \rangle$. The remaining equations of motion follow with the help of the identities

$$\langle \dot{P}^2 \rangle = 2\langle P\dot{P} \rangle , \tag{3.14a}$$

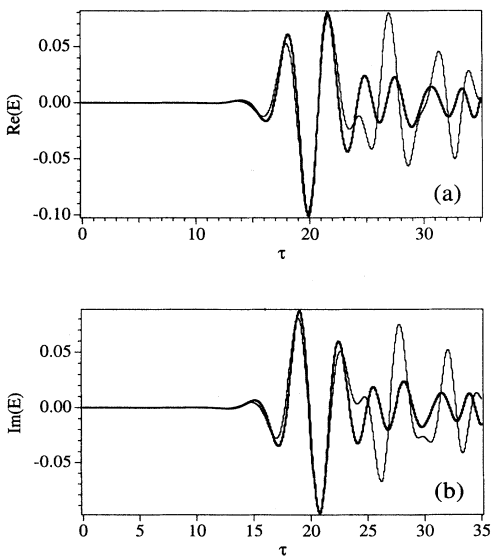

FIG. 5. Comparison between the real (a) and imaginary (b) parts of the left (thin line) and right (thick line) hand sides of Eq. (3.12a). Of the three equations (3.12) we have chosen to display the worst case. The parameters are $\Gamma = 5$, $\rho = 30$, $A_2 = 2$, $\Delta_{20} = -35$, $\Delta_{21} = 1$.

$$\langle \dot{b}^2 \rangle = -2i \langle \dot{\theta} e^{-2i\theta} \rangle \ , \tag{3.14b}$$

Finally, after simple algebraic manipulations, we arrive at the following closed set of equations of motion describing both the linear and nonlinear regime of CARL:

$$\frac{dV}{d\tau} = -iW \ , \tag{3.15a}$$

$$\frac{dW}{d\tau} = 2A_2 X - A_1 \langle S^* \rangle - 2i \langle P \rangle W - A_1^* \times [V(X+iY) + \langle S \rangle (B - V^2)] - iV \langle P^2 \rangle + 2iV \langle P \rangle^2 \ , \tag{3.15b}$$

$$\frac{dB}{d\tau} = -2i[VW - \langle P \rangle V^2 + B \langle P \rangle] \ , \tag{3.15c}$$

$$\frac{dA_1}{d\tau} = X + iY + i\Delta_{21} A_1 \ , \tag{3.15d}$$

$$\frac{dX}{d\tau} = -\frac{1}{2} Y(\langle P \rangle + 2\Delta_{20}) - \frac{i}{4}(\langle S \rangle + 3\langle S^* \rangle)(W - V\langle P \rangle) - \rho Z A_2 - \frac{1}{2}\rho A_1 \langle \Delta \rangle - X(\Gamma + i\langle P \rangle) - \frac{1}{2}\rho A_1^* [VZ + \langle \Delta \rangle (B - V^2)] \ , \tag{3.15e}$$

$$\frac{dY}{d\tau} = \frac{1}{2} X(\langle P \rangle + 2\Delta_{20}) + \frac{1}{4}(3\langle S^* \rangle - \langle S \rangle)(W - V\langle P \rangle) + i\frac{1}{2}\rho A_1 \langle \Delta \rangle - Y(\Gamma + i\langle P \rangle) - i\frac{1}{2}\rho A_1^* [VZ + \langle \Delta \rangle (B - V^2)] \ , \tag{3.15f}$$

$$\frac{dZ}{d\tau} = 4\rho A_2 X - Z(\Gamma + i\langle P \rangle) + 2\rho A_1 \langle S^* \rangle + \Gamma V - i\langle \Delta \rangle (W - V\langle P \rangle) + 2\rho A_1^* [V(X+iY) + (B - V^2)\langle S \rangle] \ , \tag{3.15g}$$

$$\frac{d}{d\tau}\langle \Delta \rangle = 2\rho [A_1^* (X+iY) + \text{c.c.}] + 2\rho A_2 (\langle S \rangle + \text{c.c.}) - \Gamma(\langle \Delta \rangle - 1) \ , \tag{3.15h}$$

$$\frac{d}{d\tau}\langle S \rangle = \frac{i}{2}\langle S \rangle (\langle P \rangle + 2\Delta_{20}) - \rho A_2 \langle \Delta \rangle - \rho A_1 Z^* - \Gamma \langle S \rangle \ , \tag{3.15i}$$

$$\frac{d}{d\tau}\langle P \rangle = -[A_1^* (X+iY) + \text{c.c.}] + A_2 (\langle S \rangle + \text{c.c.}) \ , \tag{3.15j}$$

$$\frac{d}{d\tau}\langle P^2 \rangle = 2\{-A_1^* [\langle P \rangle (X+iY) - \langle S \rangle (V\langle P \rangle - W)] + A_2 \langle P \rangle \langle S \rangle\} + \text{c.c.} \tag{3.15k}$$

We observe in passing that during a preliminary analysis of this problem, we considered a simpler alternative set of equations where we neglected the "second harmonic" contribution $B = \langle b^2 \rangle = \langle e^{-2i\theta} \rangle$; the results exhibited a far less satisfactory agreement between exact and approximate solutions, so that we abandoned further attempts along this line.

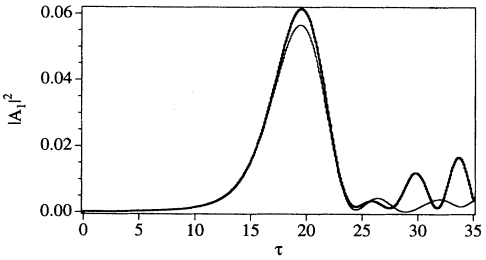

FIG. 6. Comparison between the output intensity calculated from the nonlinear collective equations (thick line) and the exact CARL equations (thin line) for the parameters used in Fig. 5.

As a test of consistency of the collective equations (3.15), we have constructed their linearized version and recovered the collective equations (2.10), as expected. It follows that the short-time behavior of the full set of nonlinear equations (3.15) matches that of the microscopic equations (2.1). With respect to the long-time behavior, in Fig. 6 we compare the output intensity calculated from the numerical integration of Eqs. (2.1) with the same quantity obtained from Eqs. (3.15). As we can see, the agreement is rather satisfactory, especially during the evolution of the first emitted pulse of CARL radiation.

IV. CONCLUSIONS

We have developed a simplified alternative description of the CARL amplification process based on a set of collective variables. While the collective equations are only approximately equivalent to the microscopic equations derived in Refs. [1,2], the agreement is rather satisfactory over a wide range of parameters where the system displays CARL gain, so that in this regime one can dispense with the lengthy numerical calculations that are required when the number of particles is large.

During the linear regime of the evolution, CARL displays gain in correspondence with the Raman peak, a feature which is common also to stationary atoms [6]. However, the inclusion of recoil in the theory brings about major qualitative modifications in the so-called Rayleigh structure of the Mollow spectrum. Not only does the symmetry of the gain profile undergo a complete change as a result of the atomic recoil, but it also indicates that the predicted evolution of the Mollow theory fails to occur in the presence of atomic recoil, to be replaced instead by the collective instability described in this paper. This can be seen most readily from Fig. 3(a) with the help of the real parts of the eigenvalues of the linearized collective equations. In fact, according to the part of the figure labeled M (the Mollow-type eigenvalues having the largest real parts) and for a sufficiently negative value of the detuning parameter Δ_{21} [for example, $\Delta_{21} \approx -50$ in Fig. 3(a)], the linearized prediction would lead to the conclusion that an initial fluctuation must be absorbed (the real part of the Mollow-type eigenvalue is negative). In the presence of recoil, however, the FEL-

type part of the same figure shows the existence of one eigenvalue with a small but positive real part. Thus, an initial fluctuation is actually amplified as a consequence of recoil-induced gain effects.

Producing a precise statement on the range of validity of the collective equations does not seem to be a simple matter. Our extensive numerical tests suggest that the agreement between the microscopic CARL equations and their collective counterparts continues to be satisfactory as long as the atomic damping rate Γ is sufficiently large and the cooling rate Γ/ρ sufficiently small, so that Eqs. (2.4) provide an accurate representation of the early stages of the evolution and that, in addition, the CARL system is reasonably above threshold.

[1] R. Bonifacio and L. De Salvo, Nucl. Instrum. Methods Phys. Res. Sec. A **341**, 360 (1994).

[2] R. Bonifacio, L. De Salvo, L. M. Narducci, and E.J. D'Angelo, Phys. Rev. A **50**, 1716 (1994).

[3] An important contribution by J. Guo, P. R. Berman, B. Dubetsky, and G. Grynberg, Phys. Rev. A **46**, 1426 (1992), contains a perturbative analysis of the effects of recoil on the response of a collection of driven two-level atoms. These authors have calculated the absorption and gain spectra of a probe field in a nearly degenerate four-wave mixing and in a pump-probe configuration and predicted the existence of new resonances whose origin could be traced to the atomic recoil.

[4] B. Bonifacio and L. De Salvo, Opt. Commun. **115**, 505 (1995).

[5] R. Bonifacio, C. Pellegrini, and L. M. Narducci, Opt. Commun. **50**, 373 (1984).

[6] See, for example, B. R. Mollow, Phys. Rev. A **5**, 1522 (1972); **5**, 2217 (1972); F. Y. Wu, S. Ezekiel, M. Ducloy, and B. R. Mollow, Phys. Rev. Lett. **38**, 1077 (1977).

[7] J. Madey, Nuovo Cimento **50**, 64 (1979); see also R. Bonifacio, G. T. Moore, M. O. Scully, and P. Meystre, Phys. Rev. A **21**, 2009 (1980).

[8] We use the term "complex bunching parameter" to avoid confusion with the traditional bunching parameter, which is the modulus of V in Eq. (3.1f).